Journal of Imaging Science and Technology® 68(3): 1–6, 2024.

Visualization of Liquid Surface Wave by Self-interference of Reflected Laser Beam with Artificial Neural Network

Yang Miao
Beijing University of Technology, College of Mechanical and Energy Engineering, China
Beijing University of Technology, Beijing Key Laboratory of Advanced Manufacturing Technology, Ping le yuan 100, Beijing, 100124, China

Silu Josue and Nihorimbere Seth
Beijing University of Technology, College of Mechanical and Energy Engineering, China

Miao Li
School of Mechatronic Engineering, Beijing Polytechnic College, Beijing, 100042, China

Xiaolu Zhang
Beijing University of Technology, College of Mechanical and Energy Engineering, China
E-mail: xiaolu.zhang@bjut.edu.cn

Abstract. *To evaluate underwater sound, a simple non-invasive optical technique based on self-interference to detect low-frequency underwater acoustic signals was demonstrated. Clear self-interference fringes of a laser beam reflected from the surface capillary wave transformed from a low-frequency underwater acoustic signal by a cylinder were observed. This study was also aimed at developing an artificial neural network (ANN) model with input from an optical pattern. The relationship between the optical pattern and the frequency of underwater sound was established, and an optimal combination of hyper-parameters was obtained. By analyzing the fringe region and the fringe interval, the frequency of the underwater acoustic signal and its relative amplitude were measured. A model based on physical optics modified the fringe distribution function, and the theoretical fit with the modified function was in good agreement with experimental observation. The BP-ANN model exhibited good performance in establishing the relationship between the optical pattern and underwater sound.*
Keywords: *ANN, underwater sound, optical detection, self-interference, air–liquid interface*

[DOI: 10.2352/J.ImagingSci.Technol.2024.68.3.030404]

1. INTRODUCTION

Effective remote and in-air optical techniques for the detection of underwater acoustic signals are of great interest for their very important applications. In principle, because of the high mass density difference between air and water, their interface may be normally considered as a perfect light-reflecting boundary with pressure release for underwater acoustic signals [1]. Therefore, the detection of light reflected from the interface might provide information about underwater acoustic signal. As per this assumption, laser sensors in the air based on light reflection were proposed for the detection of underwater acoustic signals [2, 3]. Afterward, a laser Doppler vibrometer [4, 5], lidar [6], laser beam deflector [7], and interferometry [8–10] were used for probing underwater acoustic signals. It was found that a laser beam reflected from a water surface wave appears to be diffracted. Based on this effect, the reflection technique was used to measure surface acoustic waves [11, 12]. In this way, we proposed a convenient and practical technique to detect surface acoustic waves [13]. The diffraction of the reflected laser beam was also suggested as a way to analyze underwater acoustic signals [14, 15].

In fact, the reflection of a laser beam from a liquid surface had been used to detect surface deformation caused by other factors. For example, the distorted spatial profile of a reflected laser beam was analyzed to investigate the bending of an air–water interface caused by pump light [16, 17], by solid wetting [18–22], and by drop impact [23–26]. For the curved liquid surface, we designed a visualization technique to measure the liquid surface shape and contact angle in real time [27]. We also found the self-interference fringe of the laser beam from a curved liquid surface and used the fringe to measure capillary curvature [28]. Many other optical techniques related to reflection can be used to measure liquid surface deformation such as quasi-real-time moiré reconstruction [29], background-oriented Schlieren technique [30], and image analysis interferometry [31, 32]. The light-reflection technique can be applied to a liquid surface with micron- or nanoscale curvature. A simple compact interferometer using twisted light detects picometer displacement on a liquid surface [33]. Phase interferometric particle imaging was used to measure droplet size in the micron range and size changes in nanometers [34].

Received Jan. 30, 2024; accepted for publication May 28, 2024; published online June 13, 2024. Associate Editor: Chao Liu.
1062-3701/2024/68(3)/030404/6/$25.00

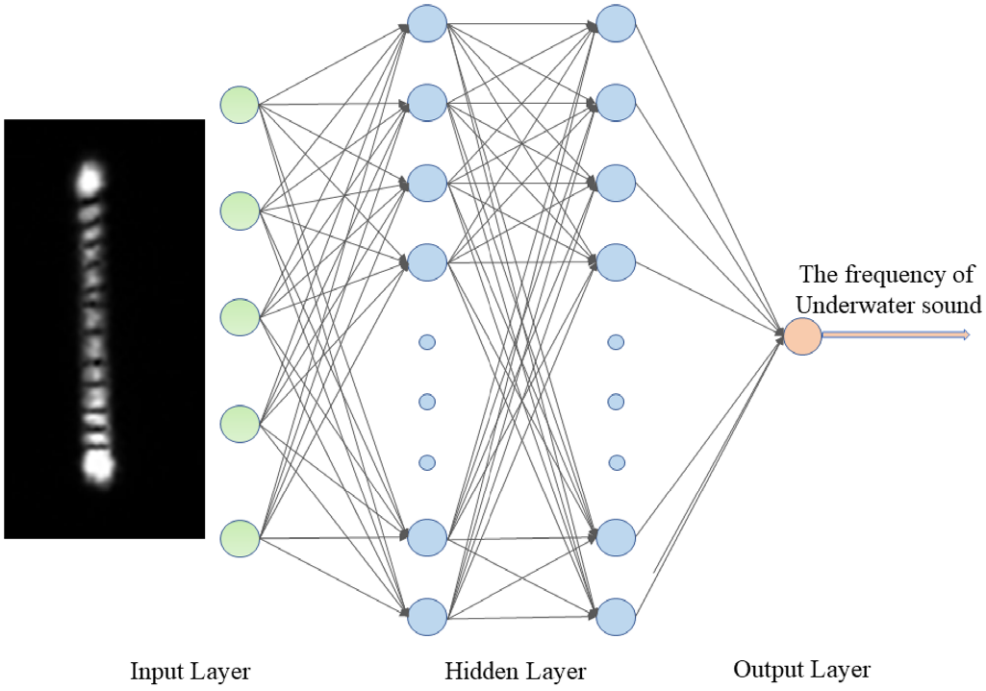

Figure 1. Schematic of BP neural network.

Artificial neural networks (ANN) are extremely versatile and have demonstrated their promising potential for modeling complex systems [35]. A novel frequency-aware neural network to synthesize consistent and detailed water surface waves from low-resolution input has been proposed [36]. The applications of two ANNs with differing structures using reflectance data generated from simulations to predict the refractive index of infiltration fluid have been reported [37]. Jörg Behler et al. introduced a first-principles quality high-dimensional neural network potential built from dispersion-corrected density functional theory (DFT) data in molecular dynamics simulations to investigate water–copper interfaces as a prototypical case [38]. The authors combined DFT, machine learning, and molecular simulations to shed additional light on the possible existence of a liquid–liquid transition in water [39]. An ANN was used to predict the normalized wetting rates for powders [40]. Furthermore, the influences of liquid surface and pattern could be treated as a black box when utilizing an ANN model to further explore the impact of various factors on the acousto-optic effect. Therefore, the ANN model may provide an effective and intuitive approach for establishing the associations between underwater sound and optical patterns.

Generally, the pressure release of underwater acoustic signal results in water surface vertical vibration, and the vibrational amplitude is in nanometers. Due to the large slosh of the water surface, it is more difficult to maintain measurement stability and eliminate background noise for the direct detection of vertical vibration. In this work, we use a cylinder to convert the surface vertical vibration caused by an underwater acoustic signal into a surface capillary wave. Clear self-interference fringes of a laser beam reflected from the surface wave are observed. The frequency and amplitude of underwater acoustic signals are measured by analyzing the fringe region and interval. Besides, the present study is aimed at constructing an ANN model for underwater sound and optical patterns with different parameters. By using a model based on physical optics and the AI model, the fringe distribution function is modified and the theoretical prediction is consistent with the experimental observation.

2. METHODOLOGY

2.1 *Acousto-optic Effect Inversion Model*

A surface capillary wave results in the self-interference fringe of the reflected laser beam. Suppose the water surface capillary wave is a simple sinusoidal wave in the illuminated area and the area just covers double wave shapes (see Figure 1). Each illuminated capillary wave shape is like a time-varying diverging mirror, which can be considered as a new light source. Because of the spatial coherence of the laser beam, the reflections from both wave shapes overlap and form interference fringes on the observation screen. Referring to Young's double slit interference, one may readily obtain the fringe intensity distribution function $I_r(\varphi)$ on the observation plane as $I_r(\varphi) = I_m(\varphi)\cos^2\{\frac{\pi\Lambda}{\lambda}[\sin\theta - \sin(\theta-\varphi)]\}$, where λ is the light wavelength, Λ is the capillary wavelength, θ is the light incident angle, and $\theta - \varphi$ describes the reflected direction. $I_m(\varphi)$ is an intensity modulation factor as in [41]; $I_m(\varphi) = \frac{1}{4\pi\left[(kA)^2 - \tan^2(\frac{\varphi}{2})\right]^{\frac{1}{2}}}$, where A and k are the amplitude

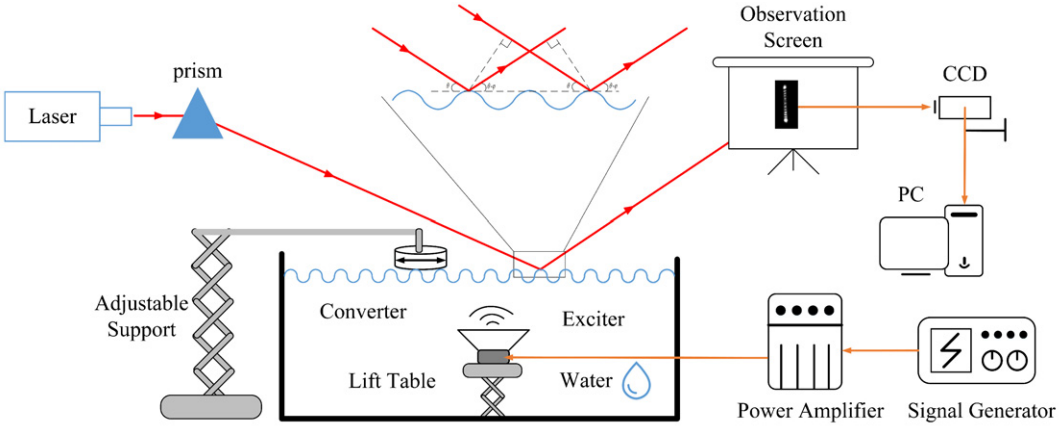

Figure 2. Schematic of experimental setup.

and the wave vector scale of the capillary wave, respectively. The expression for this modulation factor is almost consistent with the intensity distribution trend of self-interference fringes. However, for the two extremal directions, $\tan(\frac{\varphi}{2}) = \pm kA$, the intensity goes to infinity, which is obviously unreasonable.

These unreasonable extremal positions in the modulated factor should be modified. The infinite extremum results from their derivation completely based on geometrical optics. Light diffraction will occur if the laser beam is limited. There is uncertainty for the extremal direction, i.e. the azimuth φ in the extremal direction has an uncertainty Δ, which is equal to the half-width of the fringe at the extremal site. Based on physical optics, after considering this uncertainty, we modify the fringe intensity distribution function as

$$I_r(\varphi) = \frac{1}{4\pi\left[(kA)^2 - \tan^2\left(\frac{\varphi}{2}\right) + \tan^2\left(\frac{\Delta}{2}\right)\right]^{\frac{1}{2}}} \cos^2 \times \left\{\frac{\pi\Lambda}{\lambda}\left[\sin\theta - \sin(\theta - \varphi)\right]\right\}. \quad (1)$$

The intensity function is composed of two factors, the former of which is intensity modulation and the latter is fringes.

2.2 *Schematic of BP-ANN Model*

The backpropagation (BP) neural network is a multi-layer feedforward neural network where the signal propagates forward and the error propagates backward. The process of the BP neural network is mainly divided into two stages: the first stage is the forward propagation of the signal from the input layer through the hidden layer and finally to the output layer; the second stage is the backward propagation of the error from the output layer to the hidden layer and finally to the input layer. Furthermore, the weight and bias of the hidden layer to the output layer and the weight and bias of the input layer to the hidden layer can be regulated in such a process. Fig. 1 illustrates that the arrangement of input parameters follows an optical pattern. The output parameter is the frequency of underwater sound.

In this work, the sigmoid function served as the transfer function for the hidden layer while the output layer employed a purely linear function. The coefficient of determination (R^2) and the root mean square error (RMSE) between the prediction frequency and the optical pattern were adopted to assess the ANN model's performance. R^2 and RMSE can be calculated as in Eqs. (2) and (3), respectively. The minimum RMSE indicates the maximum R^2. To reduce the RMSE, each model underwent 15 rounds of training and the best-performing model was selected from them.

$$R^2 = \frac{\sum_{i=1}^{N}(p_i - m_i)^2}{\sum_{i=1}^{N}(m_i - m_{avg})^2} \quad (2)$$

$$\mathrm{RMSE} = \sqrt{\frac{\sum_{i=1}^{N}(p_i - m_i)^2}{N}}, \quad (3)$$

where m_i is the optical pattern, p_i is the prediction output, and N is the total number of all samples.

3. EXPERIMENTAL SETUP

The schematic of the experimental setup is shown in Figure 2. A signal generator and an amplifier are used to drive an underwater acoustic transducer from a few tens to hundreds of Hertz. A stainless steel cylinder with diameter 30 mm is kept on the water surface and can be precisely positioned up or down. The cylinder converts the surface disturbance caused by the underwater transducer into a surface capillary wave. A He–Ne laser (632.8 nm, 10 mW) is divided into two beams by a splitter, one of which monitors laser stability and the other illuminates the water surface at a distance 30 mm from the cylinder boundary. The incident angle of the laser beam is 1.05 rad. The illuminated area on the water surface is like an ellipse whose major axis and minor axis are about 4.8 mm and 2.4 mm, respectively. The reflected beam distribution is detected at a straight distance ($L = 5$ m) from the surface using a charge-coupled device (CCD; MER-132-30UM-L). A computer, connected to the CCD, is used to display, store, and process the reflected image.

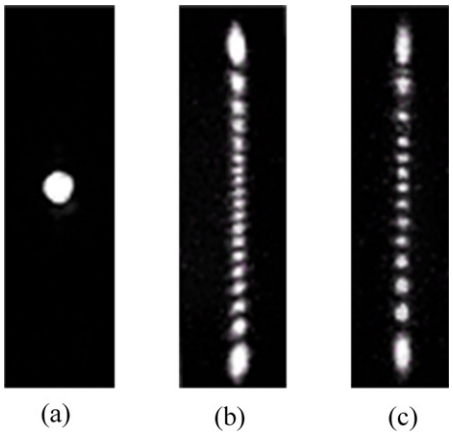

Figure 3. Self-interference fringe of the laser beam reflected from water surface disturbed by underwater transducer working at low frequency: (a) static, (b) 180 Hz, and (c) 220 Hz.

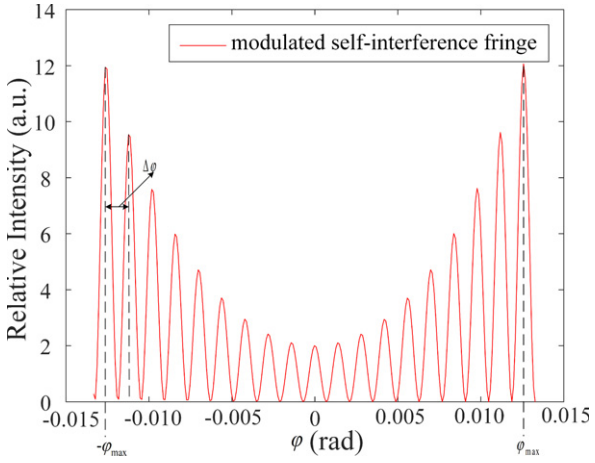

Figure 4. Simulation of self-interference fringe intensity distribution.

First, we observe light distribution on the observation screen in the case of the static water surface. The profile of the laser beam reflected from the flat surface remains undistorted (Fig. 3(a)). Second, we capture the image on the screen in the case of the transducer working. The cylinder is precisely moved downward to just touch the water surface and the generator drives the transducer to produce underwater vibration. The frequency of the generator output is 180 Hz. In the case of the disturbed surface, we observe special interference fringes (Fig. 3(b)). We define this phenomenon as self-interference because of only one incident beam in the experiment. The fringes show that their intensity is not uniform. In contrast to the usual interference fringe, the intensity is the smallest for the central fringes and reaches the maximum for the outermost side fringes. Keeping the other experimental parameters unchanged, we only tune the generator frequency to 220 Hz. The self-interference fringe (Figure 3(c)) is similar to that in Fig. 3(b) except for the fringe interval and the region size.

In the experiment, the cylinder transforms the surface vertical vibration caused by the underwater transducer into a surface capillary wave. Because the wave in bulk water is longitudinal, the underwater transducer results in the surface vibrating up and down if it is working. Because the cylinder is static, the energy of the water surface vibration under the bottom of the cylinder will only be released in the horizontal direction. Thus, the surface capillary wave is formed during the release of vibrational energy. The cylinder acts as a vibration converter, which transforms the longitudinal wave produced by the underwater transducer into a surface capillary wave. For more details, interested readers can refer to our previous work [42].

4. RESULTS AND DISCUSSION

4.1 *Performance of Acousto-optic Effect Inversion Model*

Measurements of the fringe interval and region allow us to calculate the amplitude and wavelength of the surface capillary wave. As per Eq. (1), the theoretical fit of the fringe intensity distribution corresponding to Fig. 3(b) is plotted in Figure 4. The figure shows that two fringes with maximum intensity are farthest from the center and they are located at the positions $-\varphi_{\max}$ and $\varphi_{\max}$. The interval between adjacent interference fringes is $\Delta\varphi$. All the fringes appear in the region $\{-\varphi_{\max}, \varphi_{\max}\}$. According to Eq. (1), from the intensity and fringe factors, the position $\varphi_{\max}$ and the interval $\Delta\varphi$ can be easily derived as $\varphi_{\max} = 2\arctan(kA)$ and $\Delta\varphi = \lambda/\Lambda\cos(\theta+\varphi)$. Because the angles $\varphi_{\max}$, φ, and $\Delta\varphi$ are directly measured in the experiment, the capillary wavelength Λ and amplitude A will be calculated with these formulas. The measured amplitudes and wavelengths corresponding to Fig. 3(b) and Fig. 3(c) are 2.41 mm, 2.10 mm, 4.81 μm, and 4.04 μm.

The measured frequency of the surface capillary wave can be considered as the frequency of the underwater acoustic signal. Because the surface capillary wave is excited by the underwater acoustic source, [15] proposed a mathematical model to establish the dependence of the surface capillary wave on the underwater acoustic source. It shows that only in the case where the frequency of the capillary wave is equal to that of the underwater wave, the capillary wave amplitude is significant and it is related linearly to that of the underwater acoustic wave. According to this conclusion, the frequency of underwater acoustic waves will be calculated based on the dispersion relation $\omega^2 = 8\alpha\pi^3/\rho\Lambda^3$ [24], where ω, α, ρ, and Λ are the frequency, the surface tension coefficient, the liquid density, and the measured capillary wavelength, respectively.

Meanwhile, the measured amplitude of the capillary wave can be considered as the relative intensity of the underwater acoustic wave. In the experiment, we measured the corresponding fringe region width while tuning the output power of the generator at a given frequency. The results show that the stronger the output, the larger the region of interference fringes, and the region width increases linearly with output power. This means that the amplitude of the surface capillary wave increases linearly with the intensity of the underwater signal.

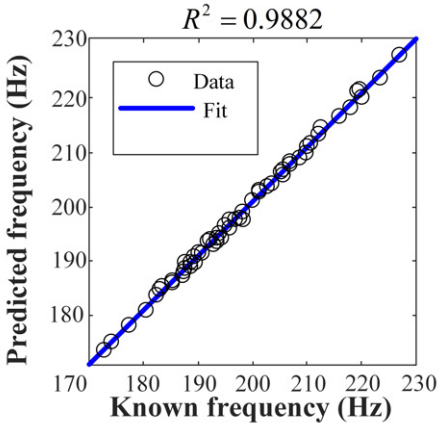

Figure 5. Scatter plot of the predicted values of frequency of underwater sound from BP-ANN with measured values.

4.2 *Performance of BP-ANN Models*

The R^2 value of the BP-ANN model for predicting the frequency of underwater sound mentioned earlier during the process was greater than 0.98 (Figure 5). Significant improvements in predicting the frequency of underwater sound from the BP-ANN model are observed compared to the physical model. This enhancement could be attributed to several factors. First, the BP-ANN model's extensive search space may contain numerous optimums. Furthermore, the predictive accuracy can be enhanced by adjusting the original thresholds and weights of the BP-ANN model.

4.3 *Limitations of the Study*

The proposed AI model established in this paper illustrated the capability to predict the frequency of underwater sound under certain conditions. Yet it imposed challenges in evaluating the frequency of underwater sound on the prediction due to the interference arising from the acousto-optic effect on liquid surface waves. Further studies may consider the effect of the depth, viscosity of liquid, or the position of underwater sound and could employ image pre-processing methods to enhance the model's capability to establish associations between the frequency of underwater sound and the optical pattern. Finally, this model can only derive the frequency of underwater sound. This underscores the necessity for future study to develop AI models capable of predicting the amplitude of underwater sound.

5. CONCLUSION

In conclusion, we have the following. (i) We have demonstrated a new and highly reconfigurable way to observe self-interference of a laser beam reflected from a water surface with a capillary wave caused by a low-frequency underwater acoustic signal. (ii) The observed self-interference fringes show that their intensity distribution is different from that of the usual fringes, and the higher the interference order, the stronger the fringe intensity. (iii) A more reasonable fringe intensity function, which is composed of the intensity modulation factor and the fringe factor, is achieved based on physical optics. The observed fringe intensity is in good agreement with this function prediction. (iv) The self-interference opens a way to detect underwater acoustic signals. A cylinder on the water surface transforms the underwater acoustic signal into a surface capillary wave, and a laser beam, reflected from the water surface with a capillary wave, forms a self-infection fringe. By analyzing the fringe region and interval directly, the relative intensity and frequency of the underwater acoustic signal are measured. The measured frequency is in the range of hundreds of Hertz and the measured wavelength of the capillary wave is in the range of a few millimeters in the experiment.

FUNDING

This work was funded by the National Natural Science Foundation of China (51975011).

REFERENCES

[1] O. A. Godin, "Anomalous transparency of water-air interface for low frequency sound," Phys. Rev. Lett. **97**, 164301 (2006).
[2] M. S. Lee, B. S. Bourgeois, S. T. Hsieh, A. B. Martinez, L. Hsu, and G. D. Hickman, "A laser sensing scheme for detection of underwater acoustic signals," Proc. IEEE **88**, 253–257 (1988).
[3] L. T. Antonelli and A. B. Fletcher, "Experimental detection and reception performance for uplink underwater acoustic communication using a remote, in-air, acousto-optic sensor," IEEE J. Ocean. Eng. **31**, 179–187 (2006).
[4] A. R. Harland, J. N. Petzing, and J. R. Tyrer, "Visualising scattering underwater acoustic fields using laser Doppler vibrometer," J. Sound Vib. **305**, 659–671 (2007).
[5] Y. F. Xu, D. M. Chen, and W. D. Zhu, "Modal parameter estimation using free response measured by a continuously scanning laser Doppler vibrometer system with application to structural damage identification," J. Sound Vib. **485**, 1–18 (2020).
[6] F. Pellen, V. Jezequel, G. Zion, and B. L. Jeune, "Detection of an underwater target through modulated lidar experiments at grazing incidence in a deep wave basin," Appl. Opt. **51**, 7690–7700 (2012).
[7] J. N. Caron and G. P. DiComo, "Frequency response of optical beam deflection by ultrasound in water," Appl. Opt. **53**, 7677–7683 (2014).
[8] O. Sasaki and H. Okazaki, "Sinusoidal phase modulating interferometry for surface," Appl. Opt. **25**, 3137–3140 (1986).
[9] A. Zhang and D. Li, "Interferometric sensor with a PGC-AD-DSM demodulation algorithm insensitive to phase modulation depth and light intensity disturbance," Appl. Opt. **57**, 7950 (2018).
[10] H. Fu, K. Wang, P. Hu, J. Tan, H. Yang, and R. Yang, "Homodyne laser vibrometer with detectability of nanoscale vibration and adaptability to reflectivity," IEEE Trans. Instrum. Meas. **69**, 542–548 (2020).
[11] B. D. Duncan, "Visualization of surface acoustic waves by means of synchronous amplitude-modulated illumination," Appl. Opt. **39**, 2888–2895 (2000).
[12] R. Miao, Z. Yang, J. Zhu, and C. Shen, "Visualization of low-frequency liquid surface acoustic waves by means of optical diffraction," Appl. Phys. Lett. **80**, 3033–3035 (2002).
[13] Y. Miao and S. Wang, "Small amplitude liquid interface sloshing process detected by optical method," Opt. Commun. **315**, 91–96 (2014).
[14] R. Miao, Y. Wang, F. Meng, and J. Ma, "Optical measurement of the liquid surface wave amplitude with different intensities of underwater acoustic signal," Opt. Commun. **313**, 285–289 (2014).
[15] Y. Ren, R. Miao, X. Su, and H. Chen, "Visualizing detecting low-frequency underwater acoustic signals by means of optical diffraction," Appl. Opt. **55**, 2018–2023 (2016).
[16] O. Emile and J. Emile, "Emile and Emile reply," Phys. Rev. Lett. **110**, 79402 (2012).
[17] G. Verma and K. P. Singh, "Universal Long-Range Nanometric Bending of Water by Light," Phys. Rev. Lett. **115**, 143902 (2015).
[18] G. Verma, J. Nair, and K. P. Singh, "low-power laser deformation of an air-liquid interface," Phys. Rev. Lett. **110**, 079401 (2013).

[19] G. Verma and K. P. Singh, "Vectorial detection of sub-microscale capillary curvature by laser beam profile," Appl. Phys. Lett. **107**, 164101 (2015).
[20] R. Miao, Z. Yang, and J. Zhu, "Critical light reflection from curved liquid interface," Opt. Commun. **218**, 199–203 (2003).
[21] J. Dong, "Visualization of the curved liquid surface by means of the optical method," J. Appl. Phys. **100**, 124914 (2006).
[22] F. Zhu, R. Miao, and Y. Zhang, "A contact angle measurement by laser glancing incidence method," J. Appl. Phys. **104**, 063112 (2008).
[23] M. S. Hanchak, M. D. Vangsness, L. W. Byrd, J. S. Ervin, and J. G. Jones, "Profile measurements of thin liquid films using reflectometry," Appl. Phys. Lett. **103**, 211607 (2013).
[24] E. Q. Li, K. R. Langley, Y. S. Tian, P. D. Hicks, and S. T. Thoroddsen, "Double contact during drop impact on a solid under reduced air pressure," Phys. Rev. Lett. **119**, 214502 (2017).
[25] M. Pack, H. Hu, D. Kim, Z. Zheng, H. A. Stone, and Y. Sun, "Failure mechanisms of air entrainment in drop impact on lubricated surfaces," Soft Matter **13**, 2402–2409 (2017).
[26] D. Daniel, J. V. I. Timonen, R. Li, S. J. Velling, M. J. Kreder, and A. Tetreault, "Origins of extreme liquid repellency on structured, flat, and lubricated hydrophobic surfaces," Phys. Rev. Lett. **120**, 244503 (2018).
[27] Y. Miao, Z. H. Qiu, Y. C. Jiang, and L. P. Hou, "Visualization of dynamic wetting by means of critical light reflection from curved liquid surface," Optik **219**, 165262 (2020).
[28] Y. Miao, Z. H. Qiu, Y. H. Jiang, X. Y. Zhang, L. Han, Z. Wang, and N. Wang, "Measuring multiscale capillary curvature using laser beam self-interference," Opt. Commun. **497**, 127149 (2021).
[29] J. Wang, V. M. Murukeshan, and A. Asundi, "A novel curvature fringe extraction method from speckle slope fringes," Optic. Commun. **205**, 43–48 (2002).
[30] N. A. Vinnichenko, A. V. Pushtaev, Y. Y. Plaksina, and A. V. Uvarov, "Measurements of liquid surface relief with moon-glade background oriented schlieren technique," Exp. Therm. Fluid Sci. **114**, 110051 (2020).
[31] S. J. Gokhale, J. L. Plawsky, P. C. Wayner, and S. DasGupta, "Inferred pressure gradient and fluid flow in a condensing sessile droplet based on the measured thickness profile," Phys. Fluids **16**, 1942–1955 (2004).
[32] G. Wiegand, K. R. Neumaier, and E. Sackmann, "Microinterferometry: Three-dimensional reconstruction of surface microtopography for thin-film and wetting studies by reflection interference contrast microscopy (RICM)," Appl. Opt. **37**, 6892–6905 (1998).
[33] G. Verma and G. Yadav, "Compact picometer-scale interferometer using twisted light," Opt. Lett. **44**, 3594–3597 (2019).
[34] Y. Wu, H. Li, M. Brunel, J. Chen, G. Gréhan, and L. Mdler, "Phase interferometric particle imaging for simultaneous measurements of evaporating micron-sized droplet and nanoscale size changes," Appl. Phys. Lett. **111**, 041905 (2017).
[35] M. Choraś and M. Pawlicki, "Intrusion detection approach based on optimised artificial neural network," Neurocomputing **452**, 705–715 (2021).
[36] C. Peng, Z. Tu, S. Qiu, C. Li, C. Wang, and H. Qin, "Learning frequency-aware convolutional neural network for spatio-temporal super-resolution water surface waves," Comput. Animat. Virtual World **6**, e2116 (2022).
[37] P. D. McAtee, S. T. Bukkapatnam, and A. Lakhtakia, "Artificial neural network to estimate the refractive index of a liquid infiltrating a chiral sculptured thin film," J. Nanophotonics **4**, 046006 (2019).
[38] S. K. Natarajan and J. Behler, "Neural network molecular dynamics simulations of solid–liquid interfaces: water at low-index copper surfaces," Phys. Chem. Chem. Phys. **41**, 28704–28725 (2016).
[39] T. E. Gartner III, L. Zhang, P. M. Piaggi, R. Car, A. Z. Panagiotopoulos, and P. G. Debenedetti, "Signatures of a liquid–liquid transition in an ab initio deep neural network model for water," Proc. Natl. Acad. Sci. **42**, 26040–26046 (2020).
[40] S. Ahadian, S. Moradian, F. Sharif, and M. Mohseni, "Application of artificial neural network (ANN) in order to predict the surface free energy of powders using the capillary rise method," Colloids Surf. A **1-3**, 280–285 (2007).
[41] R. C. Miao, X. F. Zhao, and J. Shi, "Modulated interference of reflected light from a liquid surface wave at tens Hertz frequencies," Opt. Commun. **259**, 592–597 (2006).
[42] Y. Miao, Y. Jiang, Z. Qiu, and D. Wu, "The measurement of underwater sound with optical diffraction by liquid surface wave," Eur. Phys. J. Plus **135**, 755 (2020).